Exploring Nanomechanical Properties of Materials with Atomic Force Microscopy

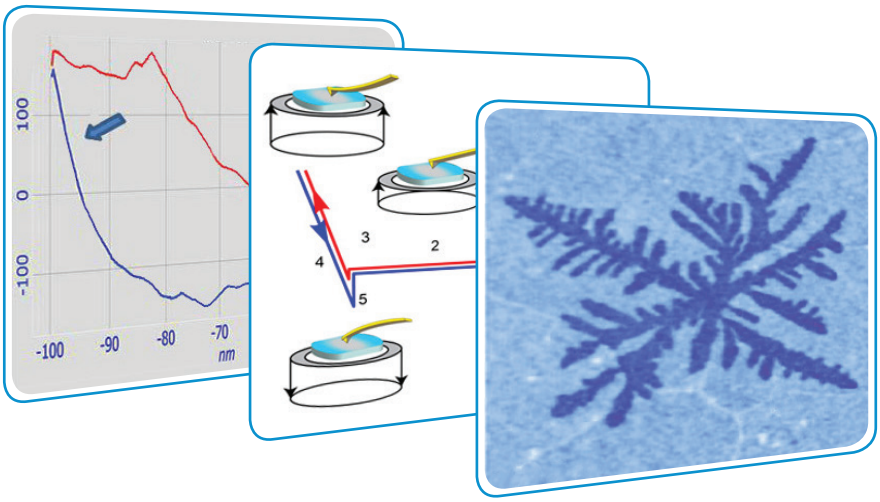

- Force effects in Atomic Force Microscopy imaging and spectroscopy
- Contact resonance, phase imaging, dissipation, and bimodal excitation
- Quantitative Atomic Force Microscopy - based nanoindentation

Sergei Magonov, NT-MDT Development

Different aspects of probing local mechanical interactions in Atomic Force Microscopy (AFM) will be discussed and demonstrated in this application note, using the practical examples obtained with the NEXT scanning probe microscope. The critical areas of study include the use of tip-sample force interactions in various modes for compositional imaging of heterogeneous materials and the quantitative examination of mechanical properties at small scales down to a few nanometers.
The application note consists of an introduction, three parts, which describe the force measurements in contact mode, in amplitude modulation (AM) mode, and in AFM-based nanoindentation, and, finally, the conclusions. The experimental data are supported by their theoretical analysis, which is based on the description of the tip-sample interactions using the Euler-Bernoulli equation and the asymptotic solutions of the oscillatory tip behavior during its interactions with a sample.

INTRODUCTION

Atomic force microscopy (AFM) was introduced to perform high-resolution imaging of surfaces for a broad range of materials [1]. Initially, this function was realized using a microfabricated cantilever with a sharp tip that scans a sample surface in contact mode. The force interactions between the probe and the sample are monitored by the deflection of the cantilever, and they are applied for profiling surface corrugations. Measurements of the tip-sample force interactions and their understanding become essential for the optimization of surface imaging [2] and, furthermore, for studies of local mechanical properties of materials [3]. Minimization of normal and lateral tip forces reduces the damage to soft samples and lowers the tip-sample contact area thus facilitating the high-resolution imaging of the topmost surface structures.

The most basic information about these interactions at a single location on a sample is obtained from force curves, which represent the dependence of the cantilever deflection on the tip-sample separation (DvZ). The schematic description of the DvZ curves and their practical examples are presented in Figures 1a-c. As the cantilever approaches a sample, attractive forces cause downward bending of the cantilever and on further movement repulsive forces start to act and bend the cantilever upwards. A strong snap of the Si probe on a Si surface, which is seen during the probe retraction in Figure 1b, is

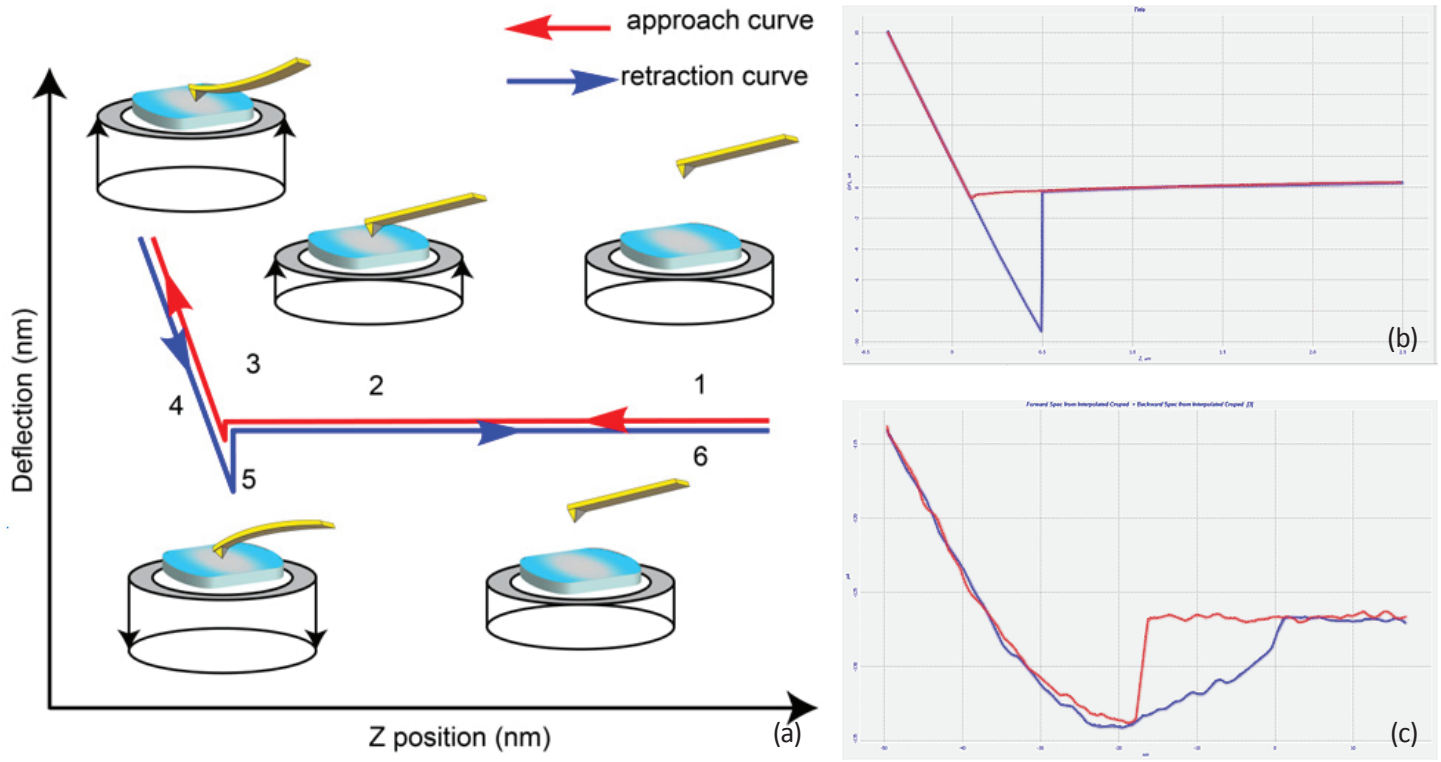

Figures 1a-c. (a) Sketch illustrating the recording of DvZ curves in AFM. In an approach (1-2-3) a sample is moved vertically by a piezo and it causes the probe upward bending in the response to the tip-force. On the way back (4-5-6) the probe reduces its bending and exercises an adhesion before leaving the sample. (b)-(c) The experimental force curves obtained, which were recorded on a Si surface and a rubber sample, emphasize the regions reflecting the sample stiffness and adhesion.

typically caused by a meniscus force originated from a water layer present on many surfaces in air. This effect is eliminated during AFM studies under water [2]. The similar region recorded in the force curve on a rubber sample, Figure 1c, looks quite different and such behavior is usually explained by adhesive tip-sample interactions. Generally, the measurements of force curves in AFM have features common to force studies with a surface force apparatus and indentation curves obtained with the stylus indenters.

The use of force curves for studies of local mechanical properties has substantially broadened AFM applications. The extreme force sensitivity of this technique has inspired a large number of deformation studies, in which pulling the probe, whose apex has been modified to stick to the sample surface, can stretch individual macromolecules. In addition to the unique force sensitivity, the small size of the probe was essential in performing both indentation and molecular pulling experiments at the nanoscale.

Typically, in AFM-based nanoindentation the DvZ curves are collected at rates in the 0.01-10 Hz range, which is well below the resonant frequency of the probes. In order to expand this single point technique to mapping the surface, the force curves are collected in a mesh of points (up to 128×128 points in an operation known as Force Volume) over the examined surface area; yet this procedure is time consuming and demands low thermal drift of the microscope. The speed of this process can be dramatically increased if only few points of the DvZ curves are collected for determination of stiffness and adhesion maps. There are also a number of dynamic approaches, such as force modulation [4], contact resonance or atomic force acoustic microscopy (AFAM) [5], which can be used for exploring the local mechanical properties in contact mode. These modes are typically applied for relatively stiff samples with an elastic modulus exceeding 1 GPa.

Several problems of contact mode imaging were overcome by the development of oscillatory modes (AM and frequency modulation – FM), in which the force interactions of the probe oscillating at its flexural resonance (30 kHz-1 MHz) are employed for AFM studies. Phase lag imaging, commonly call Phase Imaging in AM mode provides compositional mapping of multi-component polymer materials, which is primarily based on dissimilarities of local mechanical and adhesive properties of their constituents [6]. Although the phase contrast is efficient in differentiating the rubbery, glassy, and inorganic components of polymer blends, block copolymers, and composites, its interpretation in terms

of specific mechanical properties is not feasible. We will demonstrate the peculiarities of nanomechanical analysis of force curves obtained on polymer samples with AFM-based nanoindentation, which is an extension of the studies of DvZ curves where the probe deforms a sample with different loading levels. This technique can be employed with high spatial and force resolution for local nanomechanical studies of materials. Several related examples will be discussed below. We will describe different types of nanoindentation curves and the specifics of their quantitative analysis.

TIP-SAMPLE FORCES AND NANOMECHANICAL STUDIES IN CONTACT MODE

Contact mode, which was the original operation technique of the AFM, is characterized by the normal and lateral forces that act between the probe and the sample during imaging. Ideally the height images reflect the sample topography best when imaging is performed at the smallest possible force. However in practice, this is not always possible because capillary forces often strongly attract the probe to the surface and surface heterogeneities leading to tip-sample force variations outside the control of the feedback loop. The force effects in contact mode can lead to changes and irregularities in the height images; many of these effects have been recognized [7].

A more peculiar situation happens with the influence of lateral forces, as one sees from the following example. The images of a few pentacene dendritic structures of the second adlayers on top of a single pentacene layer on a Si substrate are shown in Figures 2a-d. These images were obtained using a triangular Si_3N_4 probe with a spring constant of ~ 0.06 N/m. The height and lateral force images in Figures 2a-b were recorded with the probe scanning perpendicular to the main axis of the probe. The lateral force image indicates that different parts of the dendritic structures exhibit various contrast levels compared to each other as well as to the first pentacene layer. As expected, the height profile of the entire dendritic structure is at the same level of 2 nm which corresponds to the single layer thickness of the molecules stacked with the molecular planes being perpendicular, Figure 2d. The height image, which is obtained with the probe scanning along its main axis, is quite different. Unexpectedly, part of the dendrite, which shows lower contrast in the lateral force image, appears 1-nm lower than the rest of the structure, Figure 2d. This effect might originate from variations of the lateral force that cause different degrees of probe buckling. The latter alters the apparent normal force response and therefore the related height profile. The reason for the lateral force variations can be different epitaxy between the parts of the top structure and the grain structure of the first layer that the dendrites cover [8]. An example of the dynamic mechanical studies in the contact mode (the contact resonance technique), which were performed on a surface of high-density polyethylene

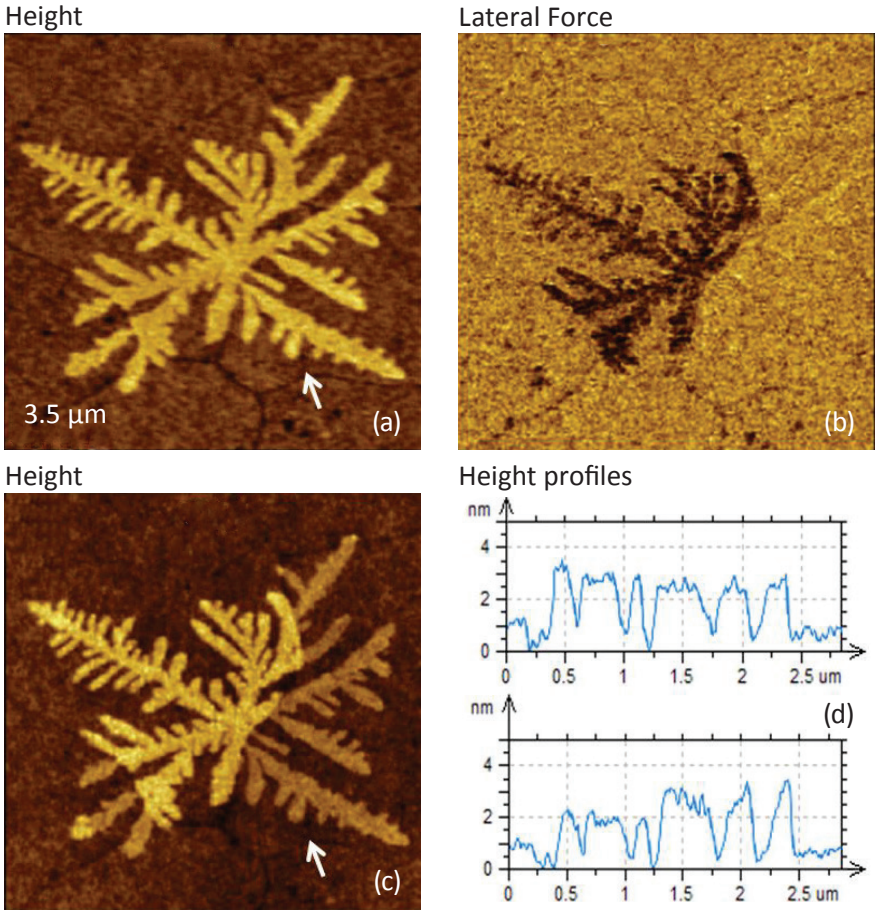

Figures 2a-d. Contact mode images on the pentacene layer with a dendritic structure atop. The height and lateral force images in (a)-(b) were obtained with a triangular Si_3N_4 probe scanning perpendicular to the probe main direction. The height image in (c) was obtained with the probe scanning along its main axis. The contrast covers the surface corrugations in the 0-5nm range in (a) and (c). The contrast in the lateral force image is in the relative units.

partially covered with a flake of graphite, is presented in Figures 3a-c. In this contact-resonance experiment a probe stays in the contact with a sample and the amplitude-versus-frequency spectrum of the probe, which is driven by a shaker, exhibits one or more contact resonances. As the probe scans over a sample surface the amplitude, phase or frequency of such resonances varies when the probe interacts with the locations of different stiffness. Basically the contact resonance shifts to higher frequency on stiffer locations.

This effect is pronounced in the amplitude and phase images shown in Figures 3b-c. An edge of the graphite flake, which is recognized in the bottom part of the examined area (Figure 3a), shows the lower amplitude values and higher phase contrast as compared to the polymer in the top region. This is consistent with the fact that graphite (elastic modulus ~ 10 GPa) is stiffer component at this location. Furthermore, the phase image also exhibits the contrast variations on the polymer surface. This effect can be attributed to local variations of either stiffness or adhesion and it demonstrates a higher sensitivity of the phase response. A continuing interest to the contact resonance studies is also related with a possibility to explore the sample viscoelastic behavior [9] and thus to enhance the characterization of local mechanical properties of materials.

PHASE IMAGING

The introduction of oscillatory AM mode substantially expanded AFM applications to soft materials such as polymers and biological specimens. The short contact time during the probe oscillation at the cantilever resonance avoids the non-desirable, destructive shearing of the sample common in contact mode. The tip-sample force interactions in AM are controlled by monitoring the amplitude of the probe, which is driven near or at its resonance, and by maintaining its damping at the desired set-point level during scanning. This operation is most common for AFM applications under ambient conditions. Control of the frequency of the oscillating probe is performed in another oscillatory mode – FM, which was originally applied in UHV but recently expanded to studies in air and under liquid. The control of the set-point amplitude in AM mode defines whether it operates in the non-contact or intermittent contact regime. The latter is characterized by an elevated level of tip-sample interactions that gives raise to substantial phase changes of the vibrating probe. Phase imaging is extremely useful in studies of multicomponent polymer materials due to its high sensitivity to variations of materials' properties, particularly, the nanomechanical and adhesive properties. However, interpretation of the phase contrast is a very complex problem. In many cases, it is impossible to establish a direct link between the phase variation and a corresponding variation in the chemical composition or specific sample properties such as adhesion, viscoelasticity, modulus, etc. Considerable difficulties for rational interpretation of the phase changes result from several factors: (i) the abrupt transition (bifurcation) from an attractive force regime to strong repulsion which acts for a short moment

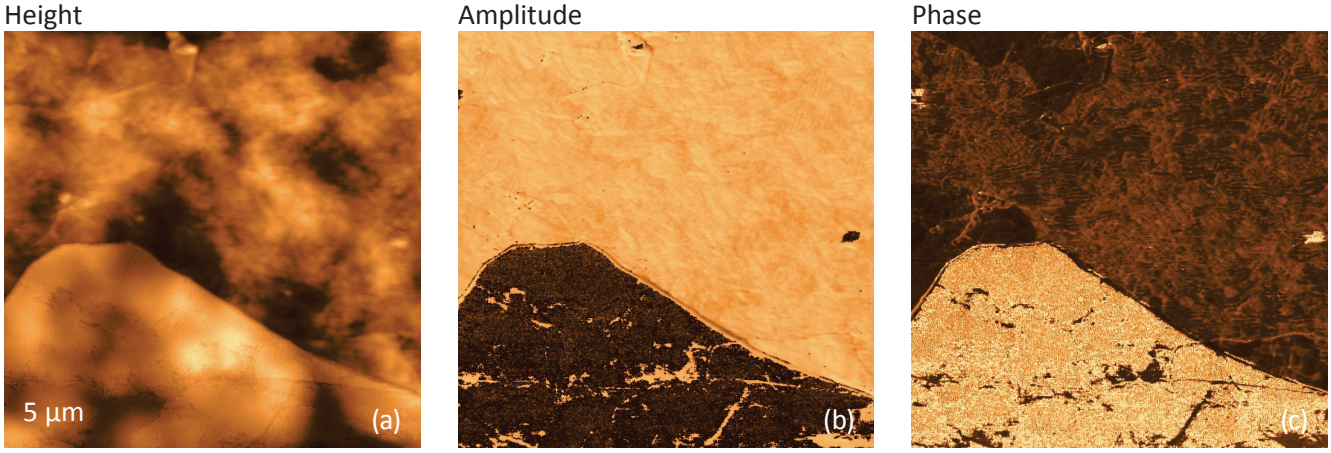

Figures 3a-c. An example of the contact resonance studies of surface of high-density polyethylene with a flake of graphite. Simultaneously recorded height image (a), amplitude image (b) and phase image (c). The amplitude and phase images were collected at the contact resonance frequency of 860 kHz for the probe with the spring constant of 4 N/m. The contrast covers the surface corrugations in the 0-50 nm range in (a) and phase changes in the 0 – 50 degrees range. The contrast in the amplitude image (b) is in the relative units.

of the oscillation period, (ii) nanoscopic localization of the tip-sample interaction, (iii) non-linear variation of both attractive forces and mechanical compliance in the repulsive regime, and (iv) the interdependence of the material properties (viscoelasticity, adhesion, friction) and scanning parameters (amplitude, frequency, cantilever position).
The interpretation of the phase and amplitude images becomes especially intricate for viscoelastic polymers.

Despite the all of the complications, phase imaging is practically important for the compositional discrimination of multicomponent polymer materials. Several semi-empirical correlations between the phase contrast and nature of individual constituents in polymer and rubber composites has been established. For example, when imaging is performed with a stiff probe (spring constant ~40 N/m) and elevated force conditions (A_0 = 50 nm, A_{sp}= 20 nm) the phase contrast changes from darkest to brightest in the following materials sequence: fillers, plastics, butyl rubber, EPDM rubber, styrene-butadiene rubber, butadiene rubber, natural rubber, oil. This succession of phase changes is valid for NEXT microscope, in which the initial phase response changes from -90 to 90 degrees passing through zero at the probe resonance. Practical examples of the phase imaging are presented in Figures 4-5.
The first example is taken from studies of a film of an immiscible blend of polystyrene (PS) and low density polyethylene (LDPE), Figures4a-d. Phase imaging at elevated forces reveals the phase separation in this blend at the microns' and submicro scales. In the large scale images, Figures 4a-b, the matrix show fine features, which can be assigned to the lamellar structure of LDPE, the round and extended blocks are smooth and, therefore, can be related to amorphous PS. This assignment is further confirmed by the phase contrast because a stiffer material (such as PS with elastic modulus in the 2-3 GPa range) typically shows a darker contrast compared to the softer (such as LDPE with elastic modulus in the 150-290 MPa range). At the smaller scale, Figures 4c-d, the phase contrast clearly shows the nanoscale domains of PS with a diameter in the 20-100 nm range, and darker linear strips (~10 nm in width) that can be assigned to the individual LDPE lamellae embedded in the softer amorphous matrix of this polymer.

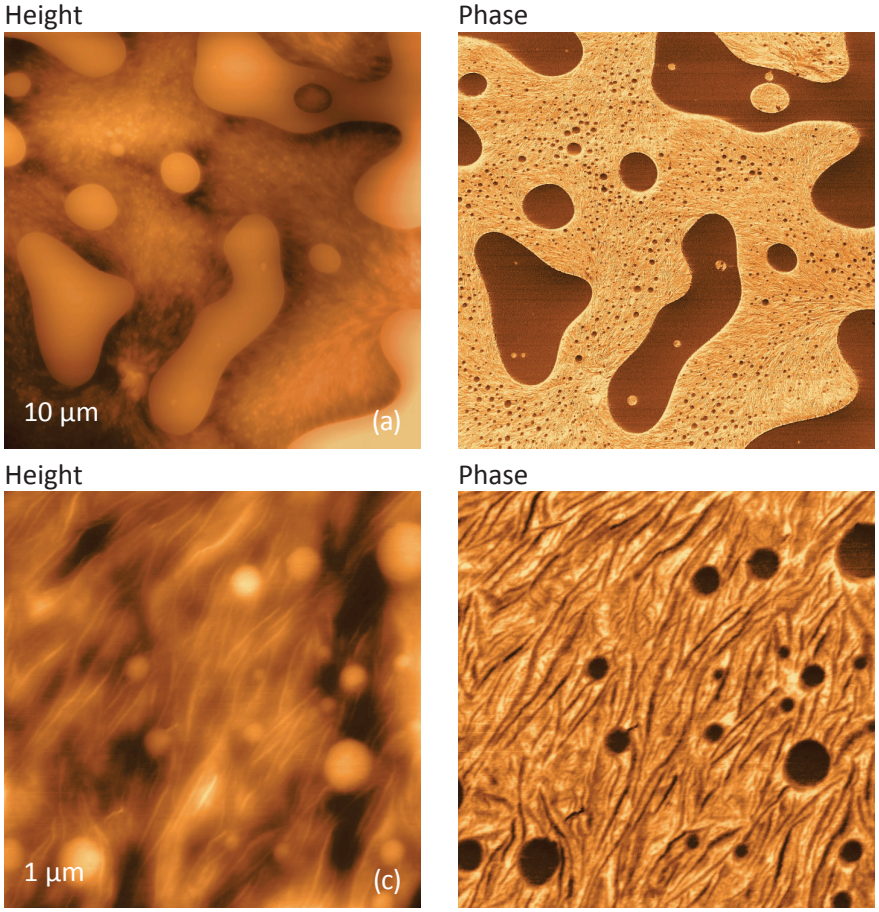

Figures 4a-d. The height and phase images of a PS-LDPE blend at two different scales. The imaging was conducted in AM mode with a stiff AFM probe (k=30 N/m) at elevated tip-force (A_{sp}= 20 nm with A_0 = 50 nm). The contrast covers the height corrugations in the 0 - 250 nm range in (a) and in the 0-30 nm range in (c). The contrast in the phase images is in the 0-95 degrees in (b) and in the 0-65 degrees in (d).

The second example, which explores the phase imaging of a binary blend of PS with poly(butadiene) – PB with a 1:1 ratio of the components,is much more complicated. The images of this blend at different scales are shown in Figures 5a-e. On the surface of the sample, its morphology is characterized by the raised round-shaped PS blocks, which are partially immersed in the PB matrix, Figure 5a.

The phase images, which were recorded at low and elevated forces (Figures 5b-c) show more heterogeneities than expected. Besides the round-like domains, a large flat area in between the domains exhibits the contrast similar to that of the PS domains. At the smaller scale, the phase image obtained at elevated force shows features with four different contrast levels.

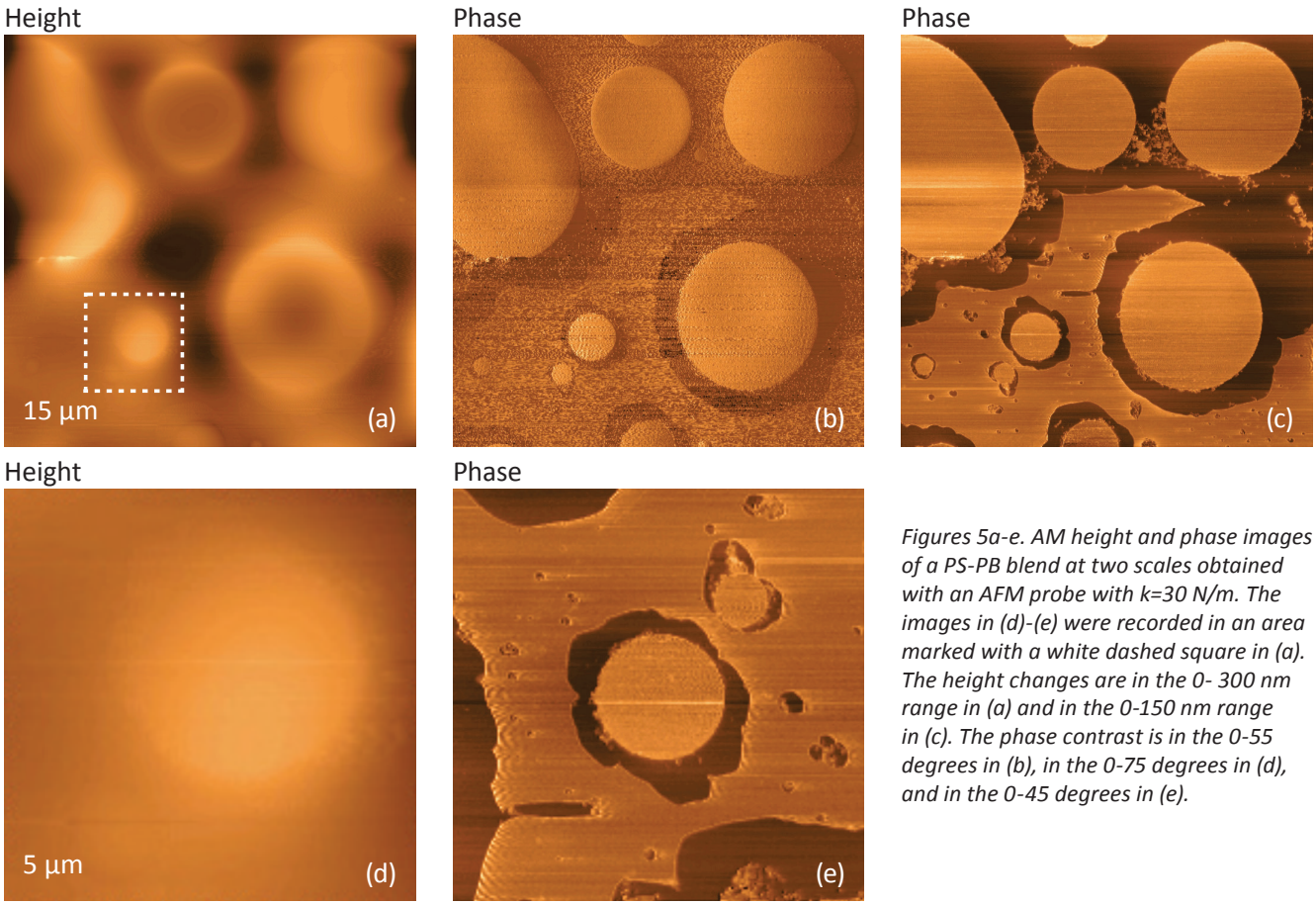

Figures 5a-e. AM height and phase images of a PS-PB blend at two scales obtained with an AFM probe with k=30 N/m. The images in (d)-(e) were recorded in an area marked with a white dashed square in (a). The height changes are in the 0- 300 nm range in (a) and in the 0-150 nm range in (c). The phase contrast is in the 0-55 degrees in (b), in the 0-75 degrees in (d), and in the 0-45 degrees in (e).

As we will see below, some of these structures can be assigned to thin layers of PS residing on the PB matrix. This example demonstrates that the phase contrast is most likely sensitive not only to the spatial variations of the mechanical properties but also to the vertical composition of the sample. Therefore, in some cases the interpretation of phase images even of binary materials is far from trivial.
The expanded capabilities of the NEXT microscopes, which incorporate several lock-in amplifiers and generators, allow studies of local mechanical properties in different less-common modes like imaging with the excitation at first two flexural resonances.

This approach was described in [10]. We have performed the similar examination of the heterogeneous polymer samples including patches of mesomorphic poly(diethylsiloxane) - PDES, which were spread on a Si substrate by rubbing. Such samples were studied with AFM previously [11] and the phase images recorded in the AM mode at elevated tip-sample forces have clear distinguished the substrates locations, amorphous and crystalline parts of PDES. Furthermore, the imaging of this sample at the 2nd flexural mode, which is ~36 times stiffer than the 1st flexural mode, made the amorphous polymer regions “invisible” in the height image due to the tip penetration through the soft material.

The examination of the PDES sample using the simultaneous drive of the probe at the 1st and 2nd flexural modes and surface tracking at the 1st flexural mode is illustrated by height and phase images in Figure 6. These images show the PDES patches, which are partially covered the substrate surfaces and aligned along the rubbing direction from the left bottom corner to the right top corner. A remarkable difference between the height and phase images is that the lamellar aggregates, which are embedded into amorphous surrounding, are exhibit much brighter phase contrast that the amorphous polymer. The same lamellar structures are barely seen in the height image. A comparison of the phase images recorded in the 1st and 2nd flexural modes shows that the phase contrast in the 2nd mode is more pronounced yet this difference is not as strong as one reported in [10]. The analytical consideration of the probe behavior when it is driven at the 1st and 2nd flexural modes shows a substantial cross-talk between the modes. Although the double excitation brings novel data this does not eliminate a need of a correct model of the tip-sample interactions for the extraction of specific mechanical properties.

The aforementioned complexity led to a strong motivation to extend the capabilities of nanomechanical studies beyond surface imaging. This inspired the development of theoretical and practical approaches to examine the dissipative and viscoelastic behavior of polymers and other materials on small scales. Here we will briefly consider the theoretical analysis of the probe behavior in AM mode. The amplitude and phase of the interacting probe are related to the mechanical forces as the tip approaches the sample and as the tip retreats from the sample (F_a and F_r) as stated by the following equations [12]:

$$\begin{cases} \sin\theta = \dfrac{1}{N}\displaystyle\int_0^{\pi}[F_a - F_r](Z_c + x\cos y)\sin y dy + \dfrac{A_{sp}^{sp}}{A_0} \\ \cos\theta = -\dfrac{1}{N}\displaystyle\int_0^{\pi}[F_a - F_r](Z_c + x\cos y)\cos y dy \end{cases}$$

where A_0 - the probe amplitude prior to its engagement into tip-sample force interactions; Z_c - an averaged position of the cantilever over a surface during oscillations, and

$$N = \frac{\pi A_0 k}{Q}$$

(k and Q - spring constant and quality factor of the probe at 1st flexural resonance). The essential parts of the equations are the integrals

$$I_{\sin} = \int_0^{\pi}[F_a - F_r](Z_c + x\cos y)\sin y dy \text{ and}$$

$$I_{\cos} = \int_0^{\pi}[F_a - F_r](Z_c + x\cos y)\cos y dy,$$

which can be connoted as the dissipative and conservation integrals, respectively.

In the case of conservative forces the dissipative integral is nullified and the first equation is simplified. A pathway from oscillatory AFM measurements to the extraction of specific material properties includes the reconstruction of the tip-sample force from the probe variables (e.g. amplitude and phase) and the calculation of the specific materials properties from the force-property model or equation.

As we have already shown [13], this task is achievable for local tip-sample electrostatic measurements because the latter are conservative and separable, in addition the electrostatic force/surface potential, electrostatic force/dielectric permittivity relationships can be derived and verified for various AFM tip-sample geometries with finite element analysis. The main hurdle on the way to the extraction of specific mechanical properties from AM measurements is poor knowledge how F_a and F_r are related to the fundamental mechanical properties such as storage and loss modulus and work of adhesion.

The use of conservative models such as Hertz, Sneddon, JKR and DMT can be justified only for true non-dissipative measurements, which are quite rare in AFM studies of polymers.

Recently [14], there was an attempt to approach studies of the non-dissipative response of polymer samples using the ratio of the dissipative and conservative integrals as follows:

$$\tan\delta_{probe} = \frac{I_{\sin}}{I_{\cos}} = \frac{\frac{A_{sp}}{A_0} - \sin\theta}{\cos\theta}$$

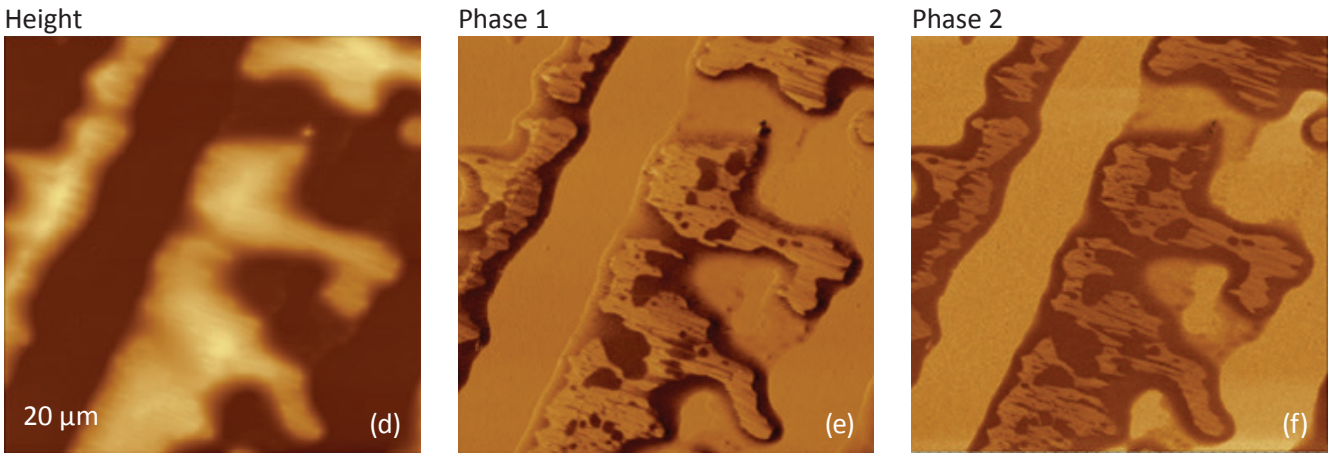

Figures 6a-c. Height and phase images recorded in the amplitude modulation mode in which the Si probe (spring constant ~ 4 N/m) was driven at the 1st and 2nd flexural modes at frequencies of 88.2 kHz and 558 kHz. The topography was examined in the 1st flexural mode and the contrast of height image covers surface corrugations in the 0-400 nm range. The phase 1 (1st flexural mode) and phase 2 (2nd flexural mode) exhibit the variations in the 0-50 degrees and 0-70 degrees ranges, respectively.

Obviously, this $\tan\delta_{probe}$ is not directly related to $\tan\delta_{sample}$, which is the ratio of loss and storage moduli determined in macroscopic dynamic mechanical measurements. Therefore, exploring the possible correlation between $\tan\delta_{probe}$ and $\tan\delta_{sample}$ needs complete practical verification, which is not trivial due to many reasons including the differences in frequencies of macroscopic and nanoscale mechanical testing. With regards to the expansion of phase imaging by addition of the dissipative and $\tan\delta_{probe}$ channels, the situation does not look very promising.

The relevant images of a sample of a binary PS/PB blend, in which the components' dispersion was improved by ultrasonic agitation, are presented in Figures 7a-d. In these images, which were obtained at elevated forces (A_{sp}= 0.5A_0, A_0 = 80 nm), the contrast of the phase, dissipation and $\tan\delta_{probe}$ channels looks quite similar.

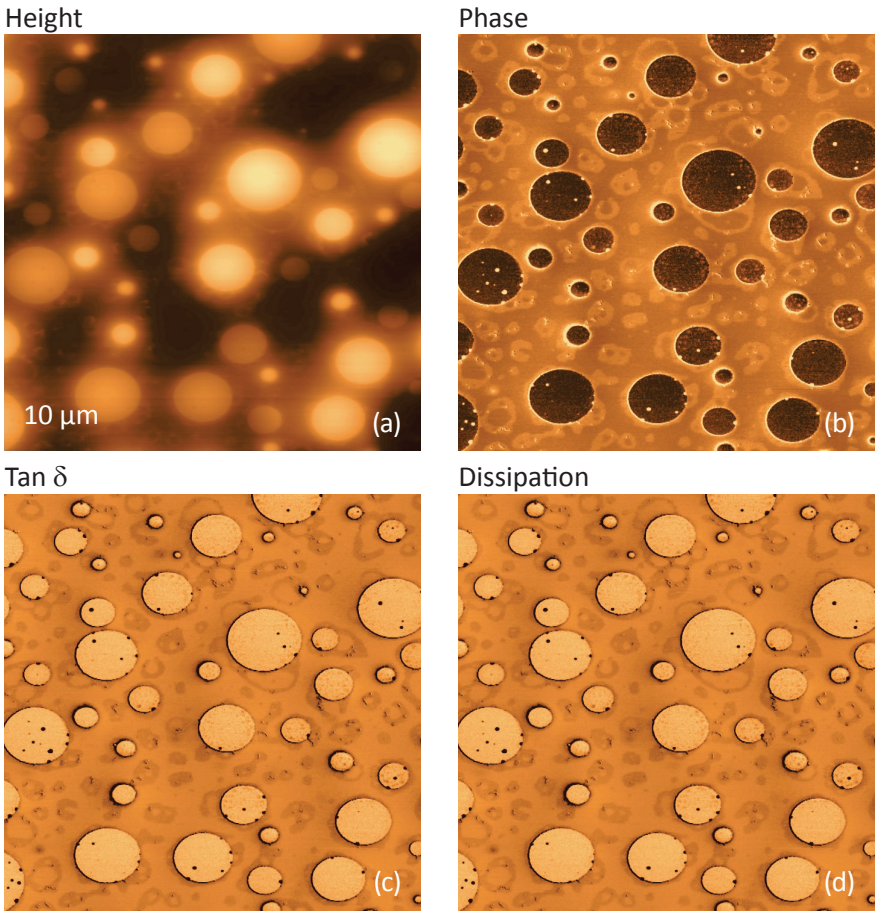

Figures 7a-d. The height, phase, dissipation and tand images of a PS-PB blend. The imaging was conducted in AM mode with stiff AFM probe (k=30 N/m) at elevated tip-force (A_{sp}=40 nm, with A_0=80 nm). The contrast covers the height corrugations in (a) in the 0-300 nm range in (a). The contrast in the phase image (b) is in the 0-55 degrees range. The contrast in the tand and dissipation images is in arbitrary units.

AFM-BASED NANOINDENTATION

The use of DvZ curves for probing of local mechanical properties in AFM was proposed more than 20 years ago [3]. Below we consider the essential elements of nanomechanical studies with AFM and present a number of illustrative examples.

The extraction of quantitative nanomechanical data from AFM measurements is a challenging task that can be achieved for a number of materials under the assumptions that a researcher can accomplish a number of requirements. The first one is related to the characterization of the AFM probe that includes the evaluation of the cantilever spring constant and shape of the tip as well as detection of the probe's optical sensitivity on a hard surface.

The spring constant of the probe is typically determined using its thermal excitation and the calculations introduced by J. Sader and coworkers [15]. The shape of the tip is best estimated from electron microscopy micrographs [16]. It can be also verified by imaging latex spheres as shown elsewhere [17-18]. The conversion of DvZ data into load-versus-penetration (PvH) curves can be accomplished by subtraction of the slope of the calibration DvZ curve obtained on hard substrate, such as the one shown in Figure 1b.

Prior to AFM-based indentation, it is quite desirable to examine the surface morphology and to choose particular locations of the sample. The imaging is accomplished in AM mode to avoid possible modification or damage of the tip and sample. For homogeneous samples, indents performed in different locations are necessary to collect sufficient DvZ curves for averaging. For heterogeneous materials preliminary imaging will allow indenting the individual components or specific locations for further comparison of their properties. It is also important to perform the measurements at different force levels by triggering the maximal probe deflection. Such

measurements can be invaluable for separation of the elastic and plastic contributions to the force curves, which will simplify their quantitative analysis. After the force curves are collected it is worth re-examining the same locations to visualize the possible indents left and to measure their shapes and dimensions.
The additional information, such as visualization of the possible pile-ups around the indents, will be invaluable in the analysis of the local mechanical properties. Finally, one should choose the appropriate deformation model for data analysis and extraction of the elastic modulus and work of adhesion. Unfortunately, most of the indentation data are analyzed with the conservative solid deformation models (Hertz, Sneddon, JKR, DMT) that discard the time-dependent (viscoelastic) effects. In some instances it can be wise to record the force curves at different rates or to follow an indents' recovery by continuous imaging in order to determine if such effects are present.

The practical examples, which illustrate the methodology of AFM-based nanoindentation, were obtained on several polymer materials with the elastic modulus in the 600 kPa – 3 GPa range.

The polymer samples include ~1 mm thick blocks of polystyrene (PS), polycarbonate (PC), Nylon 6, linear low-density polyethylene (LDPE), a blend of PS and PB, and the described earlier 4µm-thick films of semiconductor dielectric resin SiLK™ [16] and polydimethylsiloxanes (Dow Corning) with different degree of polymerization between cross-links (PDMS8, PDMS60 and PDMS130) on Si substrate [17]. These measurements were performed with a Si probe, which has a spring constant of 42.5 N/m. The tip radius, which was estimated on a latex sample [18, 19], is approximately 33 nm, which is close to the radius size (30 nm) given by the probe manufacturer. Typical DvZ curves recorded on rubbery samples are shown in Figures 8a-b. The approach and retreat curves obtained on rubbery samples of PDMS8 and PDMS130 are practically identical, and this is direct evidence of complete recovery of the sample deformation. These curves were practically the same at low and high loads. The force curves, which were recorded in 9 different locations, show remarkable consistency. Prior to the analysis of these curves they have been transformed into FvH plots, which are not much different from the DvZ plots for soft materials. Due to the conservative character of the deformation, the analysis of the force curves of PDMS8, PDMS60 and PDMS130 samples can be performed using the elasto-adhesive JKR model.

This is one of the models, which are implemented in our LabVIEW-based analysis program that was applied for the treatment of the force curves described in this note. The elastic modulus and work of adhesion data for three rubbery samples are presented in Table 1 together with the results of the macroscopic studies [18]. A comparison of these data shows a good quantitative match between elastic moduli and work of adhesion, which were obtained in the macroscopic measurements and AFM-based nanoindentation results. These findings are consistent with the earlier observations [17, 20].

The next group of polymer samples includes PS, PC and SiLK – the amorphous materials, which are in the glassy state at room temperature, and

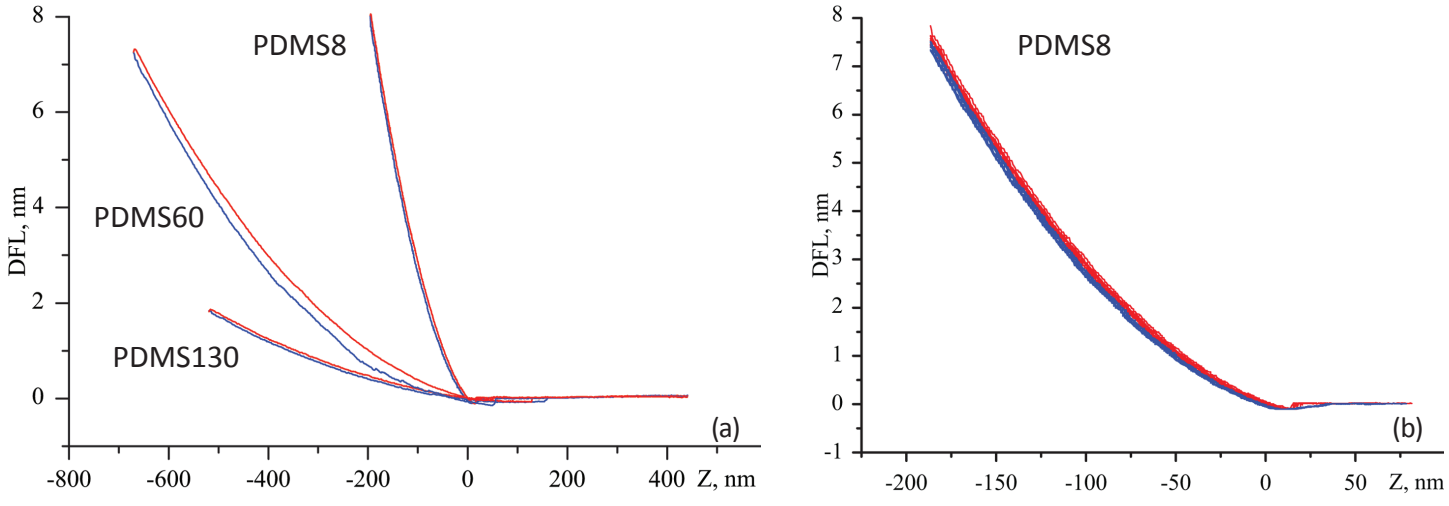

Figures 8a-b. (a) Force curves (DvZ) obtained on films of PDMS8, PDMS60 and PDMS130. (b) A set of 9 DvZ curves, which were measured in different locations of PDMS8 sample. The red curves correspond to the loading traces and blue curves correspond to the unloading traces.

Table 1. Elastic Modulus and Work of Adhesion of Rubber Films

Polymer Material	Elastic Modulus		Work of Adhesion	
	Macro	AFM	Macro	AFM
PDMS-8	13.4 MPa	13.9 MPa	49 J/m^2	32 J/m^2
PDMS-60	1.61 MPa	1.74 MPa	58 J/m^2	52.2 J/m^2
PDMS-130	0.74 MPa	0.66 MPa	47 - 58 J/m^2	42.1 J/m^2

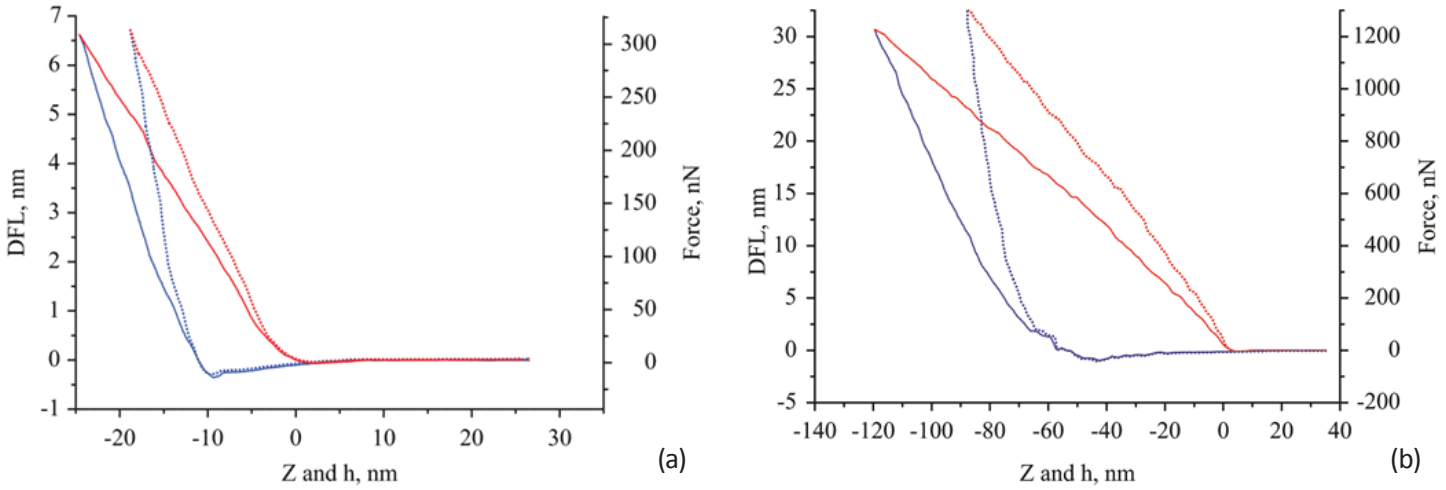

Figures 9a-b. DFL curves (solid lines) and FvH curves (dashed lines) obtained on PS surface at two different loading forces: (a) 300 nN and (b) 1.2 mN. The red-color traces correspond to the loading curves and the blue-color traces to the unloading curves.

semicrystalline LDPE and Nylon 6. We will use the force curves (DvZ and FvH) obtained on PS at different loads as a representative case, Figures 9a-b. In the contrast to the force curves of the rubber samples, the DvZ plots obtained on PS show the discrepancies between the approach (loading) and retreat (unloading) traces, which become more pronounced at high load. This behavior points out a dissipative deformation process and makes challenging the extraction of the quantitative mechanical properties.

One of the problems of the analysis is proper choice of either a loading or unloading parts of the force curves. From one side, an initial part of the loading curve, which is often used in macroscopic experiments for an extraction of elastic modulus, in AFM measurement might be influenced by surface roughness effects or surface contamination. From the other side, the use of high loads might cause a change of polymer material under the probe and, therefore, the modulus will be estimated for the deformed material. Therefore, the use of moderate loads might be optimal for AFM-based nanoindentation experiments. This suggestion is justified by the results of analysis of the FvH curves of PS, PC, LDPE and SiLK samples, which were recorded at different loads. In this analysis we neglected the dissipative character of such curves and treated them in terms of Hertz model.

The elastic moduli of the materials calculated from the force curves and, particularly, at the beginning of the unloading trace in cases of moderate loads, show a reasonable correlation with the elastic modulus values recorded in macroscopic mechanical measurements, Table 2.

Table 2. A comparison of elastic moduli of polymer materials obtained in the macroscopic studies and in AFM nanoindentation

Polymer Material	Elastic Modulus	
	Macro	Macro
LDPE	152 - 290 MPa	204 MPa
PC	1.79 - 3.24 GPa	2.30 GPa
PS	3.0 - 3.5 GPa	2.99 GPa
SiLK	2.45 GPa	2.25 GPa

When the load is increased the dissipative character of the curves becomes more pronounced and this might be one reason that the use of the solid state deformation models, which do not account for materials plasticity and viscoelasticity, does not usually provide rational results. In many cases, however, the analysis of FvH curves obtained at high loads showed reasonable elastic moduli when the unloading traces were treated in terms of Sneddon model with plastic correlation [16].

The important feature of AFM-based nanoindentation is that the indented locations can be visualized with high special resolution in the resultant images. The surface areas of PS, PC, SiLK and HDPE with the indentation marks, which we left by the AFM probe that deformed the samples with ~ 3µN load, are shown in Figures 10a-d. The cross-section profiles, which were drawn in the vertical direction along the central row of the indents, are shown together with the height images.

One can notice that high pile-ups are formed around the indents left in PS sample due to its plasticity, and they are practically absent in case of LDPE. Regarding the indent depth, it is the largest for the softer LDPE and the smallest for SiLK. The latter fact indicates a fast recovery of tip-induced deformation in this dielectric resin. Therefore, time-dependent effects should be taken into consideration during analysis of mechanical response of SiLK sample.

The comparison of the indents made in different polymers shows that we can learn much about local mechanical properties of polymers in addition to the measurements of elastic modulus and adhesion. This statement is further supported by the indenting results, which were obtained a surface of an ultrathin film of a binary blend of PS and poly(vinyl acetate) - PVAC, Figures11a-b, and on lamellar structure of high-density polyethylene (HDPE), Figures 11c-d. Two grids of 9 indents are seen on the round-shape domain of PVAC and surrounding matrix of PS. Although, at room temperature these components are in glassy state and elastic modulus of PS is slightly larger than that of PVAC the phase image shows a darker contrast on the PVAC domains.

The contrast is difficult to interpret because of an additional complication related to the fact that

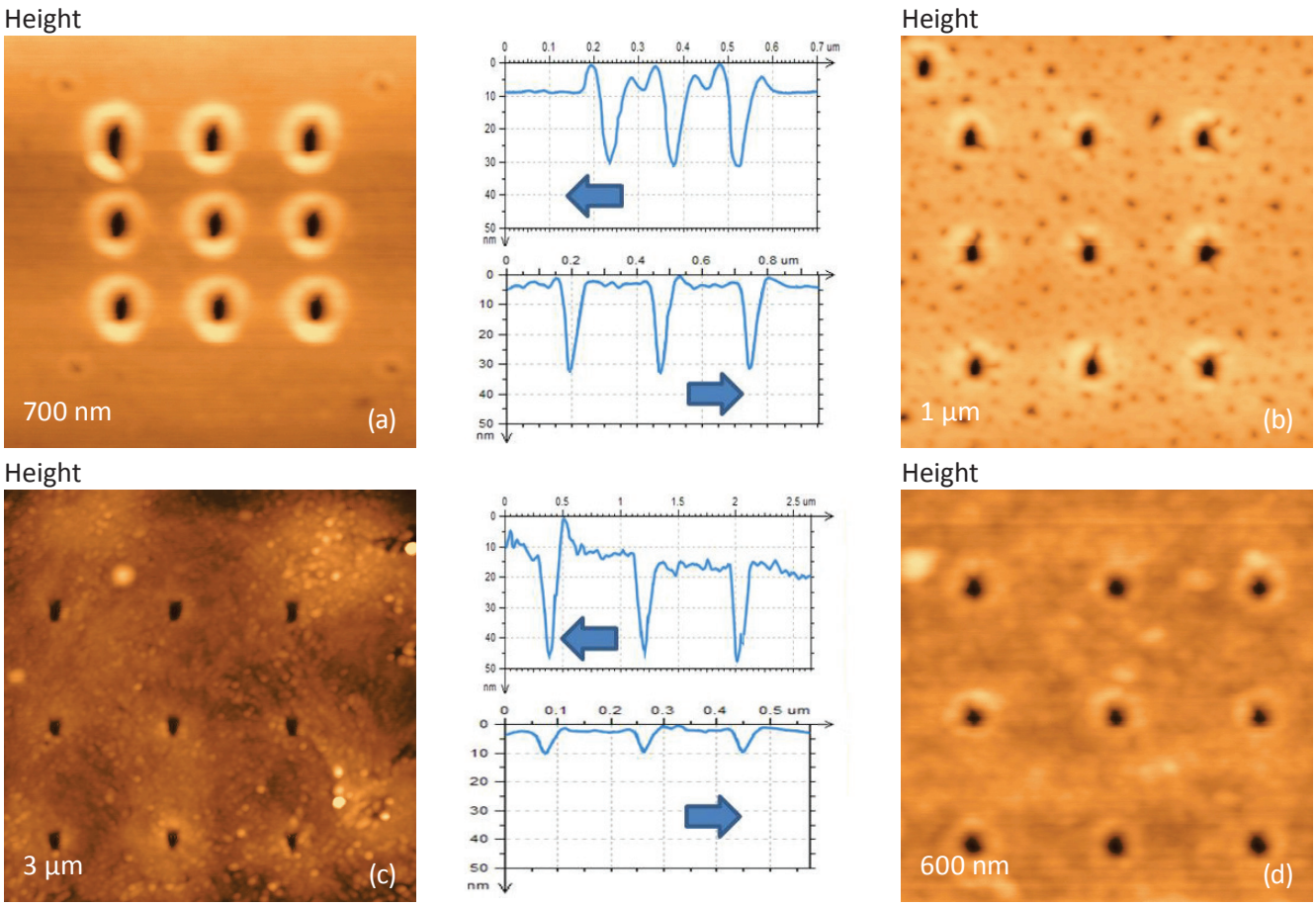

Figures 10a-d. Height images of the indents left on surfaces of different polymers: PS (a), PC (b), LDPE (c) and SiLK (d) with the probe (spring constant 42.5 N/m, tip radius of 33 nm) acting at 1.2 µN force.The cross-section profiles, which were taken along the indents of the central columns, are shown in between the images.

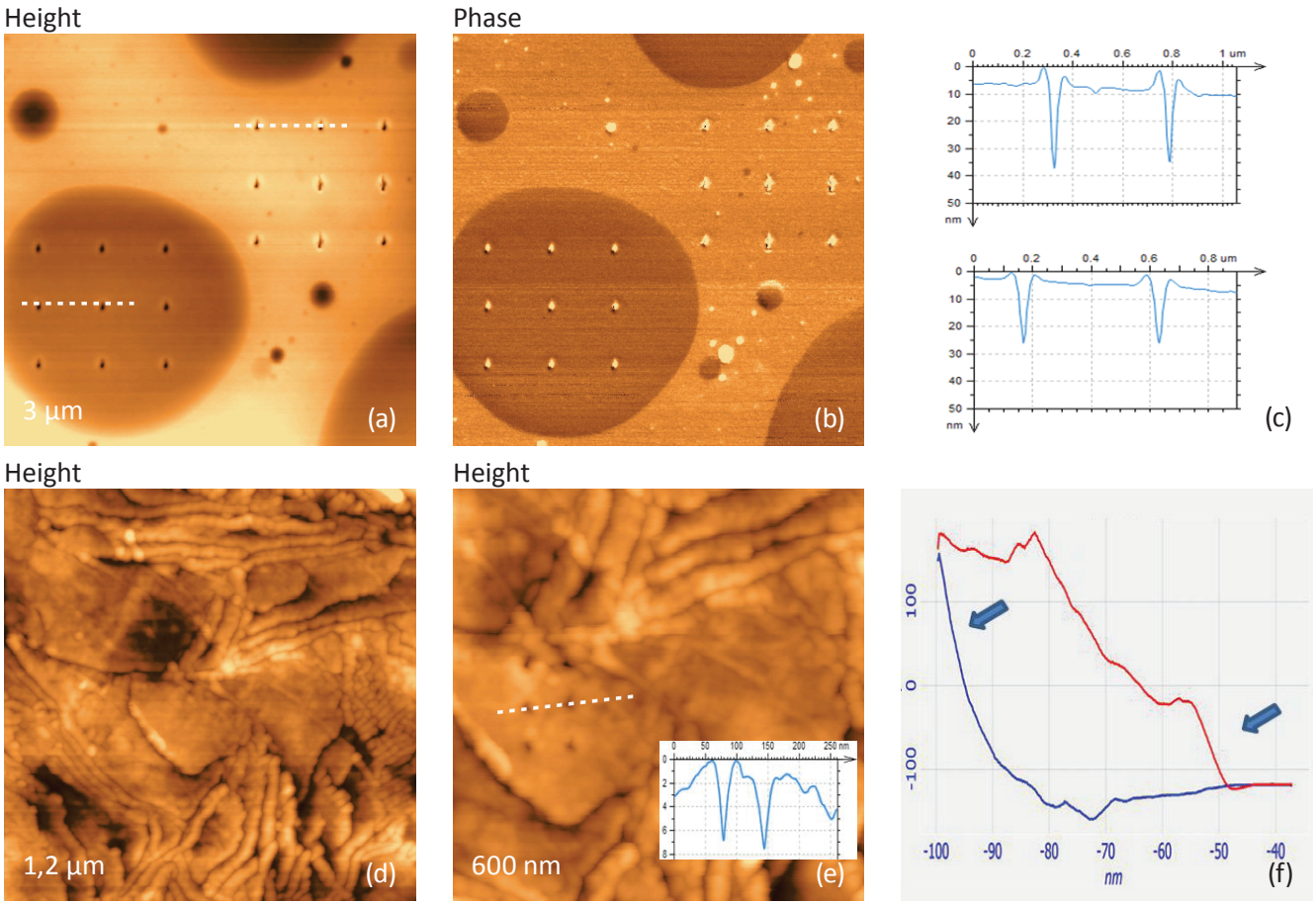

Figures 11a-f. (a)-(b) Height and phase images of a film of binary blend PS/PVAC with two grids of the indents made with the regular Si probe (spring constant 40 N/m). The cross-sections along the indents, which were taken along the directions marked with the white dashed lines in (a) and (b), are presented in (c). (d)-(e) Height images of the lamellar structures of HDPE with the smaller image taken at the location where a flat-lying lamellae was indented in a 2´3 grid. The cross-section along two indents in a direction marked with a white dashed line is shown in the insert in (e). The force curve (DvZ) recorded during one of the indentation event is shown in (f). The red curve corresponds to the loading trace and the blue curve – to the unloading trace. The blue arrows indicate the parts of loading and unloading curves, which were used for the estimation of elastic moduli.

a rigid substrate might influence the local thicknessof such 70-nm thick film. A comparison of the indents appearance and the cross-sections, which are presented in Figure 10c, points out that the matrix material is more plastic whereas the PVAC indents are smaller most likely due to their faster recovery.

Another example is taken from studies of HDPE sample, whose surface exhibits developed lamellar structures with the individual lamellae being flat or edge-on oriented, Figure 11d. Several indents were made on flat-lying lamellae, and the remaining indents of 6-7 nm in depth are shown in Figure 11e. These values are close to the thickness of individual lamellae that was most likely penetrated by the tip. The loading and unloading traces recorded during the indenting of the lamellae (Figure 11f) are rather complicated.

At the beginning of the loading path, which is indicated with a blue arrow, the deformation is elastic and it transforms into a small plastic part before climbing further. The initial deformation is quite similar to one that was reported in the indenting of the flat lamellae of the ultra-long alkane $C_{390}H_{782}$ [21]. The unloading portion looks more typical for deformation of semi-crystalline polymers. The estimates of the elastic modulus for the loading and unloading paths in the regions indicated with the arrows showed that the elastic modulus of the initial deformation at least 50% higher.

This can be expected because the polymer chains are oriented vertically in the flat-lying lamellae and exhibit higher modulus compared to the bulk material with random orientation of polymer molecules.This example demonstrates the unique ability of AFM in studies of mechanical properties of the confined nanostructures.

The variety of 2D and 3D morphologies of polymer materials is enormous and some of them are non-trivial for characterization. Even in binary blends their constituents can appear in

structures of different size and shape as shown in phase image of PS/PB blend, Figure 12a.

As we learned earlier (see the description of Figures 5), the bright domains of the phase image can be assigned to PS structures embedded into PB matrix. Several locations, which are marked with small circles of different colors, were chosen for the indentation experiments, and the phase image obtained after the experiments is presented in Figure 12b. Surprisingly, the DvZ curves obtained at the "blue" and "green" locations, which are assigned to PS and PB materials, are the same, Figure 12c. The loading and unloading paths show mostly strong adhesion.

The phase image in Figure 12b, which shows a circle of PB at the former "blue" location, allows us to suggest that the PS domain was quite thin and was destroyed by the tip, which was attracted to the sample because of its relatively large size. The DvZ curves, which were obtained at small and large round-shaped islands of PS, have different shapes, Figures 12d-e.

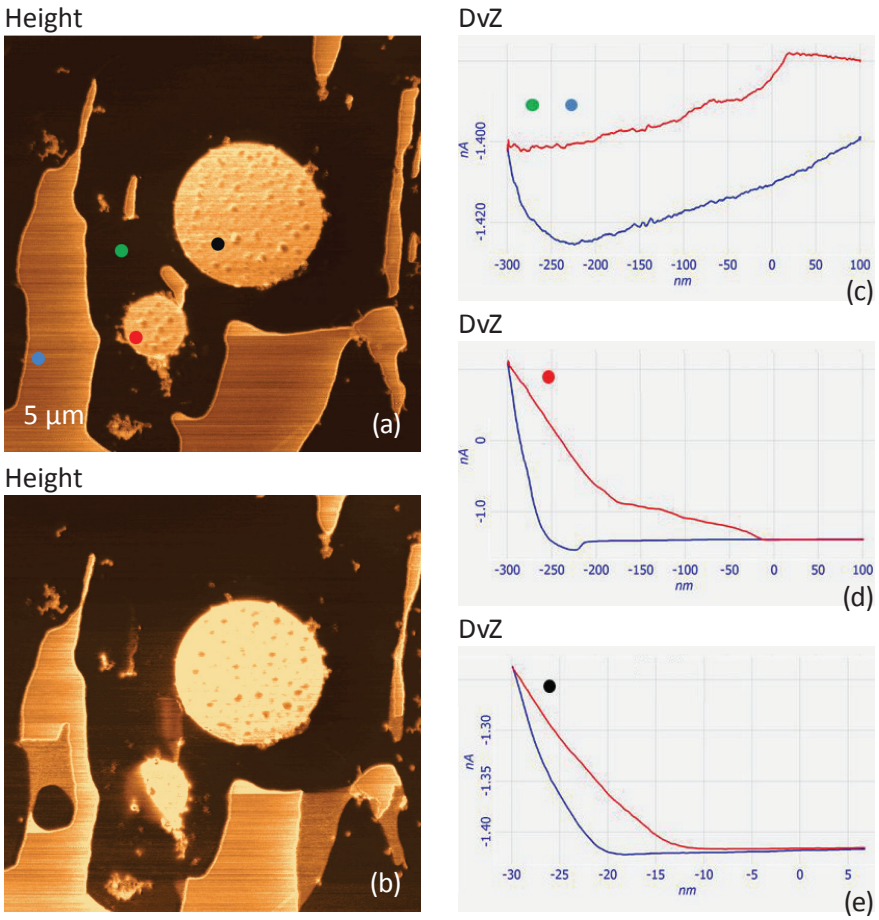

Figures 12a-e. The phase images of the surface of a film of PB/PS blend are shown prior the indentation probing in several locations marked with the color circles (a) and after the indentations (b). DvZ curves, which were recorded during indentation of the color-coded locations, are presented in (c) – (e).

The curve obtained on the small island has two stages (Figure 12d) and this might correlate with a partial damage of the island as seen from the phase image in Figure 12b. The curve, which was collected on the black-colored location of the big island, looks common to those collected on the blocks of PS and other amorphous polymers. This example of the sample complexity shows that a comprehensive study of multicomponent materials can be quite difficult and likely requires the interplay between different methods and approaches.

In further development of the nanoscale mechanical measurements with AFM techniques there is a novel trend in data analysis - a transition from non-dissipative models to more sophisticated approaches accounting for viscoelasticity effects. As we mentioned before, the time-dependent effects strongly manifest themselves in the recovery of the indents [22-23].

This effect is illustrated by imaging of the indents, which were left on a surface of a block prepared from a binary blend of polyethylenes with different degree of octene branching. The constituents of the blend have different densities (0.92 g/cm^{-3} and 0.86 g/cm^{-3}) and crystallinity. The surface of the sample is enriched in low-density material and does not show lamellar morphology.

The sub-surface morphology might be very different and can exhibit itself in the nanoindentation experiments, and particularly, in the indent recovery pattern. This is demonstrated in the height images and the related graph in Figures 13a-d. The first two images were recorded 5 and 20 minutes after the indentation experiment, in which a grid of 9 surface imprints was made. The imprints disappeared slowly and became almost invisible in the height image (Figure 13c), which was recorded 10 hours after the image in Figure 13b. The analysis of the images shows the different recovery kinetics for the imprints, with the slowest for the indent in the center, Figure 13d.

The time changes of the imprint profile hint at the affine character of the recovery similar to the finding in the experiments on styrene-butadiene copolymers [24]. In the same paper, it was shown that the depth of the imprint follows the variations of the corresponding homogeneous creep-recovery experiment. Therefore, by imaging the imprint one can obtain the variations of the polymer compliance function. This example shows that local mechanical properties of polymers and other materials can be examined in different AFM-based experiments with the choice of the most appropriate mode.

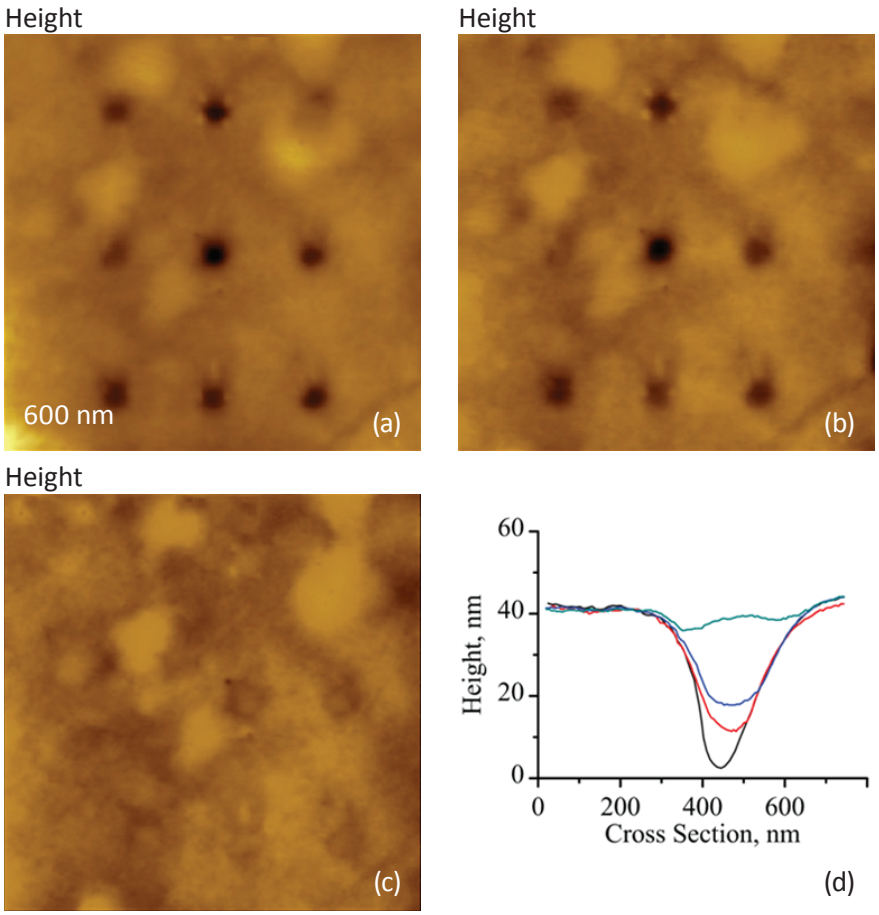

Figures 13a-d. Height images of the location of a binary polyethylene blend with the components having densities of 0.92g/cm-3 and 0.86g/cm-3 with the indentation imprints. The image in (a) was obtained 5 minutes after the indentation procedure, the image in (b) was recorded 20 minutes after the image in (a) and the image in (c) – 10 hours after the image in (b). (d) Cross-sectional traces (black, red, dark blue and light blue) across the central imprint were taken in the images, which were recordedrespectively 5, 25, 40 minutes and 10.5 hours after the indentation.

CONCLUSIONS

The tip-force mechanical interactions are the core of AFM and they manifest themselves in different modes and operation conditions. Therefore, knowledge of the tip-force effects is indispensable for the correct interpretation of AFM data and for their use for the exploring local mechanical properties of materials.

Several techniques for probing of sample's stiffness and adhesion were illustrated on practical examples obtained with the NEXT microscope, which is equipped with most of the common modes for studies of mechanical properties. The differences in mechanical properties of the materials are employed for compositional imaging of multi-component samples in contact resonance mode and for phase imaging in AM mode. AFM nanoindentation is a technique that provides the local nanomechanical data that for some polymer materials can be used for extracting the quantitative elastic modulus and work of adhesion.

However, broader acceptance of this method is limited by the restrictions for the solid-state, non-dissipative models used for data analysis. Several time-dependent effects in local mechanical studies were presented to underline the need for their serious consideration. A development of novel models accounting the plastic and viscoelastic behavior of polymersis essential for the further progress of AFM nanomechanical studies.

REFERENCES

1. G. Binnig, C. F. Quate, and Ch. Gerber “Atomic force microscope” Phys. Rev. Lett. 1986, 56, 930–933.
2. A. L. Weisenhorn, P. Maivald, H.-J. Butt, and P. K. Hansma “Measuring adhesion, attraction, and repulsion between surfaces in liquids with an atomic force microscope” Phys. Rev. B. 1992, 45, 11226-11232.
3. N. A. Burnham, and R. J. Colton “Measuring the nanomechanical properties and surface forces of materials using an atomic force microscope” J. Vac. Sci. Technol. A 1989, 7, 2906–2913.
4. P. Maivald, H. J. Butt, S. A. C. Gould, C. B. Prater, B. Drake, J. A. Gurley, V. B. Elings, and P. K. Hansma, “Using force modulation to image surface elasticities with the atomic force microscope” Nanotechnology 2, 103-106, 1991.
5. U. Rabe, S. Amelio, M. K.-M. S. Hirsekorn, M. Kempf, M. Göken, and W. Arnold “Imaging and measurement of local mechanical material properties by atomic force acoustic microscopy” Surf. Interface Anal. 2002, 33, 65-70.
6. S. N. Magonov “AFM in Analysis of Polymers” Encyclopedia of Analytical Chemistry, (R. A. Meyers, Ed.), pp. 7432-7491, John Willey & Sons Ltd, Chichester, 2000.
7. M. Bai, S. Trogisch, S. Magonov and H. Taub “Explanation and correction of false step heights in amplitude modulation atomic force microscopy measurements on alkane films” Ultramicroscopy2008, 108, 946-952.
8. V. Kalihari, D. J. Ellison, G. Haugstad, and C. B. Frisbie “Observation of unusual homoepitaxy in ultrathin layers of pentacene films and correlation with surface electrostatic potential” Adv. Mater. 2009, 21, 1-7.
9. P. A. Yuya, D. C. Hurley, and J. A. Turner, “Contact Resonance Atomic Force Microscopy for Viscoelasticity” J. Appl. Phys.2008,104, 074916-22.
10. N. F. Martinez, S. Patil, J. R. Lozano, and R. Garcia “Enhanced compositional sensitivity in atomic force microscopy by the excitation of the first two flexural modes” Appl. Phys. Lett. 2006, 89, 153115-7
11. S. N. Magonov, V. Elings, and V. Papkov “AFM study of thermotropic structural transitions of poly(diethylsiloxane)” Polymer 1997, 38, 297-307.
12. S. Belikov, and S. Magonov “Classification of Dynamic Atomic Force Microscopy Control Modes Based on Asymptotic Nonlinear Mechanics” Proceedings American Control Society, St. Louis, 979-985, 2009.
13. “Exploring materials with AFM-based electric modes” NT-MDT Application Note. 2012.
14. R. Proksch, and D. G. Yablon “Loss tangent imaging: Theory and simulations of repulsive-mode tapping atomic force microscopy” Appl. Phys. Lett. 2012, 100, 07106-07109.
15. J. E. Sader, J. W. M. Chon, and P. Mulvaney “Calibration of rectangular atomic force microscope cantilevers” Rew. Sci. Instrum.1999, 70, 3967-3969.
16. S. Belikov, N. Erina, L. Huang, C. Su, C. Prater, S. Magonov, V. Ginzburg, B. McIntyre, H. Lakrout, and G. Meyers “Parametrization of atomic force microscopy tip shape models for quantitative nanomechanical measurements” J. Vac. Sci. Technol. B2009, 27, 984-992.
17. S. Belikov et al “Theoretical modeling and implementation of elastic modulus measurement at the nanoscale using atomic force microscope” J. of Physics: Conf. Series 2007, 61, 1303-1307.
18. C. Odin, J.P. Aime, Z. El Kaakour, and T. Bouhacina “Tip’s finite size effects on atomic force microscopy in the contact mode: simple geometrical considerations for rapid estimation of apex radius and tip angle based on the study of polystyrene latex balls” Surf. Sci.1994, 317, 321-340.
19. “NEXT Scanning Probe Microscope: Visualization of Surface Nanostructures and Morphology” 2012, NT-MDT Application Note 086.
20. H. Lakrout “Quantitative AFM-Based Nanoindentation of Poly(dimethyl siloxane) Films” Proc. Of Annual Meeting of the Adhesion Soc., 31st, 2008, pp.292-294.
21. S. Magonov “High-Resolution Visualization and Compositional Analysis of Polymers with Atomic Force Microscopy” Int. Journ. Polym. Analysis and Characterization, 2011,16, 508-518.
22. S. N. Magonov and D. Reneker “Characterization of Polymer Surfaces with Atomic Force Microscopy” Annul. Revs. Mat. Sci.1997, 175-222.
23. S. Magonov, J. Alexander, and S. Belikov “Exploring surfaces of materials with atomic force microscopy” in “Nanoscale applications for information and energy systems. Nanoscience and technology” A. Korkin and D.J. Lockwood (eds). Chapter 7, Springer, New York, 2012, in press.
24. C. Basire, and C. Fretigny “Étude locale des propriétés d’adhésion de matériauxviscoélastiques avec un microscope à force atomique” C. R. Acad. Sci. Paris 1997, 325, 211-220.